Taylored Taylor Vortices

Sarah Macumber
Advisors: Michael Sprague, Henry Tufo, Patrick Weidman

May 9th 2005

Abstract

Using the canonical Taylor-Couette problem, and other known results, we verify the correctness of a parallel spectral element code for axisymmetric incompressible fluid flow. We then demonstrate how one can tailor the appearence of vortices in the classical Taylor-Couette annulus by alterations on the interior cylinder's geometry. We find that we can make vortices appear of different magnitude and wavelength, and that we can force them to appear anywhere we like by introducing a discontinuous notch in the interior cylinder. Theoretically we should be able to produce steady flow and unsteady flow in different regimes by this methodology. However, we find that the Ekman pumping caused by our discontinuity does not allow for Taylor Vortex Flow and stable Circular Couette Flow to exist simultaneously. While we can represent any discontinuous configuration we like, we find that the magnitude of the vortices, as a function of radius ratio, have a large part in the actual physical visualization of our tailored vortices. This study of discontinuous geometries will be useful in furthering the application of Taylor-Couette study in real world situations.

Contents

1 Introduction

Fluid instabilities are not easily captured in numerical models. Taylor's experiment in 1923 was a major intellectual breakthrough, representing the first case of a stability calculation quantitatively matching experimental values. Taylor examined incompressible flow in an axisymmetric concentric annulus configuration, and found that if the rotation speed of the inner cylinder is greater than a critical value, the circular-Couette flow (CCF) becomes unstable to axisymmetric perturbations. The axial and radial motion of the fluid forms pairs of toroidal vortices, now known as Taylor-vortex flow (TVF). If the inner cylinder is driven even faster this flow becomes unstable to non-axisymmetric perturbations producing azimuthal waves in the Taylor vortices. This instability can be characterized by a non-dimensional parameter known as the Reynolds number. Because the behavior of Taylor-Couette vortices is so well known, the rotating cylinder apparatus has become fundamental to the study of instability and nonlinear behavior. "The Taylor-Couette system of shear flow in concentric cylinders is a canonical system that provides valuable insight into centrifugal stability of rotating flows as well as low dimension bifurcation phenomina" [4]. It is now commonly used for quantitative comparison between theory and experiments.

Interesting experiments have been done regarding the effects of endwalls, heat and hydromagnetics on TVF. In experimentation, the finite length of the annulus introduces endwall effects known as Ekman boundary layers. These endwall effects interact with the centrifugal instability and the subsequent wavy vortex flow causing TVF below the theoretical critical Reynolds number[4]. If the fluid is radially heated or heated from an end-cap then the Taylor-Couette system can be used to study turbulent Rayleigh-Bénard convection. The Taylor-Couette system can also be applied to study the interaction of magnetic fields and electrically conducting liquids or gases. Recently, A. P. Willis and C. F. Barenghi developed a formulation of the governing magnetohydrodynamic (MHD) equations of the cylindrical Couette geometry, suitable for time stepping in the nonlinear regime [8]. Other applications of the Taylor-Couette annuli include reaction vessels viscometry, cooling of rotating electrical machinery, dynamic filtration and classification, electrolytic applications and catalytic chemical reactors.

The aim of this paper is to investigate the effect of the interior cylinder having irregular geometries. Work on irregular geometries has been previously explored. In 1926, not long after Taylor's experiment, Terada and Hattori [6] experimentally studied flow stability for a variety of inner/outer noncircular cylinder arrangements. Later, more work was done to characterize the bifurcations to TVF for these geometries. Simulations have been done with a circular spinning inner cylinder and an elliptical stationary outer cylinder, showing that increasing ellipticity destabilizes the flow and increasing eccentricity stabilizes the flow [3]. Mullen [2] and Snyder [5] began studying the flows between noncircular containers in the late 60's. In 1987 Lewis [1] derived the base flow for the case of a rotating cylinder and a stationary square outer container.

2 Model Problem

In this paper we will be using a parallel spectral element code to simulate the flow in discontinuous axisymmetric geometries. Before we can do that we must first consider the well known established results for flow in continuous geometries. Hence, we will examine the model problem of Taylor-Couette flow in continuous concentric cylinders. We will verify the correctness of the code using the classical Taylor Couette problem and other known results. Thus, we begin with a discussion of the geometry, governing equations and the numerical model.

2.1 Geometry

The classical annulus configuration is shown below in figure (2.1). In non-dimensional terms, the variable radius of the interior cylinder is given as r_1, and the radius of the exterior is given as r_2, and the cylinder is of height h. The stability of the flow can be characterized by the ratio of the two radii $\eta = r_1/r_2$ and the Reynolds number Re. The Reynolds number $Re = \frac{\Omega R_1 d}{\nu}$ is a function of gap width $d = r_2 - r_1$, rotational rate of the interior cylinder Ω and the kinematic viscosity ν. For subcritical Reynolds numbers $Re < Re_c$, stable circular Couette flow sets up in the annulus. For supercritical Reynolds numbers $Re > Re_c$ Taylor vortices set up with period λ.

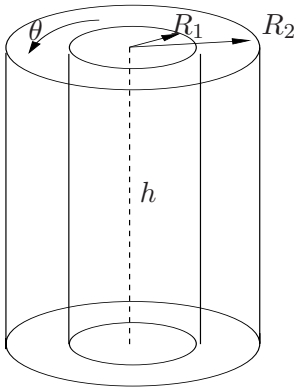

Figure 1: Concentric Cylinder Geometry

2.2 Governing Equations for Taylor-Couette Flow

In cylindrical coordinates (r, z, θ) we non-dimensionalize with the following characteristic scales: velocity $(u_r^*, u_\theta^*, u_z^*)$ with ΩR_1, spatial coordinates (r^*, z^*) with $d = R_2 - R_1$, pressure p^* with $\rho\Omega^2 R_1^2$ and time t^* with $\frac{d}{\Omega R_1}$ to obtain the non-dimensional axisymmetric Navier-Stokes equations for incompressible flow,

$$\begin{aligned}
\frac{\partial u_r}{\partial t} + (\mathbf{u}\cdot\nabla)u_r - \frac{(u_\theta)^2}{r} &= -\frac{\partial p}{\partial r} + \frac{1}{Re}\left(\nabla^2 u_r - \frac{u_r}{r^2}\right) \\
\frac{\partial u_\theta}{\partial t} + (\mathbf{u}\cdot\nabla)u_\theta + \frac{u_r u_\theta}{r} &= \frac{1}{Re}\left(\nabla^2 u_\theta - \frac{u_\theta}{r^2}\right) \\
\frac{\partial u_z}{\partial t} + (\mathbf{u}\cdot\nabla)u_z &= -\frac{\partial p}{\partial z} + \frac{1}{Re}\left(\nabla^2 u_z\right)
\end{aligned} \tag{1}$$

where

$$(\mathbf{u}\cdot\nabla) = u_r\frac{\partial}{\partial r} + u_z\frac{\partial}{\partial z}$$

$$\nabla^2 = \frac{1}{r}\frac{\partial}{\partial r}\left(r\frac{\partial}{\partial r}\right) + \frac{\partial^2}{\partial z^2}$$

where the Reynolds number is given as $Re = \frac{\Omega R_1 d}{\nu}$. These are the governing equations we will solve.

3 A Parallel Spectral Element Code

3.1 Nek5000

In this thesis, the simulation package Nek5000 is used to model axisymmetric flow in an annulus. Nek5000 is a package authored by Paul Fischer, Lee Ho, Einar Ronquist and Henry Tufo. Nek5000 is a parallel spectral element code which simulates time-dependent incompressible fluid flow and heat transfer in both stationary and time-dependent geometries. The Nek5000 package consists of three computer codes: PRENEK, NEKTON and POSTNEK. PRENEK is a preprocessor in which the user inputs the geometry (mesh), physical (boundary and initial conditions) and numerical parameters (i/o , solvers, etc) of the particular simulation. Then, solutions are computed using the parallel spectral element code NEKTON. NEXTON returns the fluid velocity $\mathbf{u} = (u_r, u_\theta, u_z)$, the pressure p, the temperature T, passive scalars given by the user and in the case of time-dependent geometry the mesh velocity $\mathbf{w} = (w_r, w_\theta, w_z)$. These results can then be examined in the post processor POSTNEK, which allows the user to graph and visualize the results. There are various implementations of the spectral element method (SEM) available for use. The method, developed by Patera, couples the efficiency of global spectral methods with the geometric flexibility of finite elements [7]. We will discuss the general SEM method and summarize details of the code as relevant to this thesis. For further details see the complete manual [7].

3.2 Spatial Discretization

Nek5000 tessellates the spatial domain into non-overlapping quadrangles in which the solution, data and geometry are approximated by high-order polynomial expansions. Some methods use triangles instead of quadrangles because they are more appropriate to complicated geometries. However, triangular elements are more computationally intensive than quadrangles which make use of the tensor product in computing fast derivatives. Another reason Nek5000 uses quadrangles is that methods which use triangular elements often restrict the order of polynomial refinement because of computational cost.

The interpolating polynomials in Nek5000 are a nodal basis set constructed using Lagrange-Legendre polynomials with roots at Gauss-Lobatto quadrature points. As seen in figure(3.2) the points cluster near element boundaries. A nodal basis set is used in Nek5000 because Gauss-Lobatto quadrature results naturally in diagonal matrices which enables fast tensor-product techniques to be used for iterative matrix solution methods. Some SEM methods use a hierarchical modal basis set, therefore increasing the polynomial refinement from $O(N)$ to $O(N+1)$ is equivalent to the addition of the $O(N+1)$ polynomial. This would make it easy to vary polynomial refinement from element to element. However, in Nek5000 one must recompute the nodal basis functions in order to change the order of the SEM. Thus Nek5000 uses the same interpolation order for all elements.

Within each element the time-dependent variables (v, p, T), are expanded in (N-1)th order Lagrangian interpolants through the Gauss-Lobatto Legendre collection points. For example, temperature is expanded $T = \sum_i T_i h_i$, where h_i are the Lagrangian polynomials that are unity at the ith Gauss-Lobatto node and zero at all others. Errors can be reduced exponentially by increasing the order of the interpolates or linearly by increasing the number of elements. For problems having smooth solutions, such as the incompressible Navier-Stokes equations, exponential convergence is obtained with increasing polynomial order, despite the fact that only C^0 continuity is enforced across element interfaces [7].

Note that since NEK5000 is intended to solve large problems, it never forms the global or elemental matrices explicitly. Meshing can be done inside of PRENEK or with the fortran code

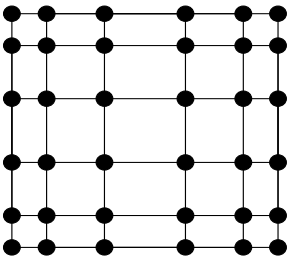

Figure 2: Example of Reference Element for Gauss-Lobatto points for polynomial order $N = 6$

genbox. Nek5000 also supports time-dependent geometries. Details of meshing can be found in the user manual [7].

3.3 Temporal Discretization

In NEKTON, convective terms like velocity and temperature are solved in a semi-explicit time-dependent evolution, meaning only data from the previous time step is used in the integration of these terms. This is done to avoid having to solve a nonlinaer, nonsymmetric system of algebreic equations at each time step. The implicit terms, like pressure, are solved on a staggered grid with an implicit scheme. Due to the explicit treatment of the convective terms, a restriction on the time step $\triangle t$ must be enforced for stability. The stability restriction, referred to as the Courant condition, is

$$\triangle t < C min_{D_F} \{ \frac{\triangle r}{|u_r|}, \frac{\triangle \theta}{|u_\theta|}, \frac{\triangle z}{|u_z|} \}$$

where C is the Courant number, the numerators are the distances between the points and the denominators are the magnitudes of the velocities. However, there is no restriction on the time step for the implicit terms. Thus, Nek5000 advances the implicit terms with large time steps and then sub-cycles the explicit terms on smaller time steps. Unless given explicity, NEKTON automatically calculates the sub-cylces based on the stability requirements imposed by the Courant condition and the implicit time step.

time stepping is done with a Pth order Adams-Bashforth (AB) multistep scheme for $P = 1, 2, 3$. In our simulations, we found that the first order method is not sufficiently accurate at high polynomial and mesh refinements. The third order method tends to excite high modes, and without a high-pass filter, it tends to add energy into the system, increasing error. Thus, in this investigation we use the second order AB method because it was found to be the most stable and was recommended by P. Fisher. Unfortunately, in the axisymmetric case, we are unable to use NEKTON's automatic time stepping because of the way we model u_θ. Essentially, we use a passive scalar to model u_θ (see the section on 3D solutions in 2D) which is not included in the Courant calculation. Thus, in all of our simulations we use a fixed time step without the method of characteristics. If we find our runs to be unstable, we simply reduce the time step. The steady-state solutions were achieved by NEKTON as the time-dependent-asymptotic result of a transient calculation.

3.4 Diffusion and Pressure terms

The diffusion terms and the pressure/incompressibility condition are treated implicitly using a Mth order Backwards Differentiation multistep scheme. There is no time restriction on these terms and they result in a large linear system of equations which is solved with an elliptic Helmholtz solver which is based on the conjugate gradient method. For the explicit (convective) terms, there

is not matrix inversion, only matrix-vector multiplication. Matrix inversion is avoided by using an additive scheme which does inversion on each individual element. The pressure terms are solved on a staggered grid as shown below in figure(3.4). This is done to reduce the size of the pressure matrix and to avoid messy boundary conditions by keeping the pressure terms on the interior of the grid.

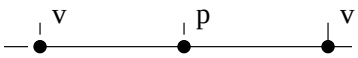

Figure 3: Example of Staggered Pressure Grid

3.5 3D solutions in 2D

For efficiency, we use NEKTON to interpret a two-dimensional Cartesian geometry as the cross section of a three-dimensional axisymmetric body, with the translation $(x, y) \rightarrow (z, r)$. In NEKTON, axisymmetric flows are assumed to have no azimuthal velocity. Because of this, we have to add an additional equation to represent the missing u_θ terms. See the appendix for details as to how to implement this in NEKTON.

4 Validation

By using well known results we can validate using Nek5000 for solving the axisymmetric Navier-Stokes equations in cylindrical coordinates. Linear stability analysis allows us to solve for the steady-state circular Couette flow. A derivation of the steady-state velocities can be found in the appendix. This flow becomes unstable to axisymetric perturbations at a certain critical Reynolds number. Based upon asymptotic expansions we can therefore perturb the flow with $O(\epsilon)$ noise terms. These perturbations decay for the subcritical case $Re < Re_c$ and grow to Taylor Vortices for the supercritical case $Re > Re_c$. It was therefore important to control any numerical errors which could lead to perturbations larger than $O(\epsilon)$. Large perturbations could cause the flow to bifurcate to an incorrect steady-state solution. In order to control numerical orders, it was necessary to determine appropriate discretizations in time and space along with appropriate polynomial refinement. Analysis of appropriate discretization is done by simulating both cylinders of finite and infinite length.

4.1 Annulus of infinite length

We use the simulation of an infinite cylinder to verify the well known relationship between the radius ratios and the critical Reynolds number. We define the origin at $z = 0$ at the bottom of the inner cylinder and for a nondimensional height h. By writing R_1 and R_2 in terms of $\eta = R_1/R_2$,

$$R_1 = \frac{\eta}{1-\eta}, \quad R_2 = \frac{1}{1-\eta}$$

we can define the boundary conditions and initial conditions solely in terms of η.

4.1.1 Boundary Conditions

The no-slip boundary conditions and initial conditions are defined in terms of $\eta = R_1/R_2$. Since we have axisymmetric flow,

$$u_r(r, z, \theta) = u_z(r, z, \theta) = 0, \qquad \text{for all } r, z, \theta$$

To simulate an infinite cylinder we use periodic boundary conditions on the end caps,

$$u_\theta(z = 0) = u_\theta(z = h), \qquad \frac{\eta}{1-\eta} \leq r \leq \frac{1}{1-\eta}$$

The outer cylinder is stationary,

$$u_\theta = 0, \qquad r = \frac{1}{1-\eta} \quad 0 \le z \le h$$

For the interior cylinder we specify Dirichlet boundary conditions.

$$u_\theta = 1, \qquad r \le \frac{1}{1-\eta} \quad 0 \le z \le h$$

4.1.2 Initial Conditions

The initial conditions are used to set up the steady-state subcritical CCF in the annulus. The equation for CCF comes froms solving the Navier-Stokes equations when $\frac{\partial u_\theta}{\partial t} = 0$ (see appendix). This base flow is then perturbed with $O(\epsilon)$ random noise so that we can make observations as to the stability of the flow at a particular Re.

$$u_\theta = \frac{\eta}{1+\eta}\left[\frac{1}{(1-\eta)^2 r} - r\right] + noise$$

4.1.3 Simulations

In order to verify that the onset of instability occurred at the correct Reynolds number the steady-state solution was perturbed and observations were made on the growth or decay of those perturbations. Those observations where then compared to numerical solutions of the Reynolds number and wavelength as a function of the radius ratio which can be derived through linear stability analysis (Provided by P. Tagg, see appendix). Using NEKTON we were able to place bounds, $0.99Re_c < Re < 1.01Re_c$, on the Reynolds number for a given η with 1% error. We also verified the correct wavelengths. This was done for several values of η, including values in the regime for which $Re_c \to \infty$

For these simulations the height of the cylinder was taken to be the wavelength associated with the particular η. The majority of these simulations were run with meshes containing evenly spaced elements. However, one can see that the initial radial velocity profile becomes increasingly non-linear as η decreases. Thus, for small η values it was important to refine the mesh near the interior cylinder to capture the sharp changes in radial velocity. In these cases a graded mesh was used to cluster more small square elements near the rotating wall. Because of the symmetry, temporal and polynomial refinement where much more significant to the accuracy of the result than spatial refinement. On average, 9th degree polynomials and $O(.01)$ time steps were more than enough accuracy for the method when the average area of an element was $O(.1)$ on a grid which had an area of $O(10)$.

The following plots are offered as validation of the numerical method and discritization scheme. In the following plots $\eta = .75$. In figures (4) and (5) we can see that below Re_c $O(\epsilon)$ perturbations decay and above Re_c $O(\epsilon)$ perturbations grow resulting in Taylor Vortical flow. We know that we have an appropriate discretization in time and an appropriate order of polynomial refinement because in figure (7) is it easy to see that refining the discritization past $N = 9$ and $DT = .01$ does not affect the steady-state solution. In figure (6) we confirm that the Taylor vortices have the appropriate wavelength.

Using this methodology, we were able to verify that the steady-state solution was captured and that transience into vortical flow occurred at the correct Reynolds number for several values of η.

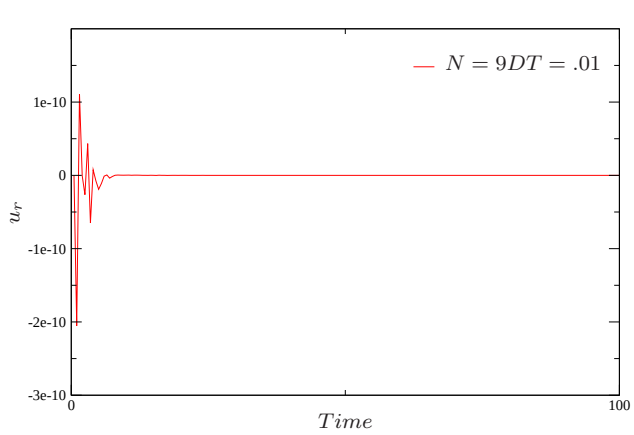

Figure 4: Subcritical u_r, $\eta = .75 \quad Re = .99Re_c$

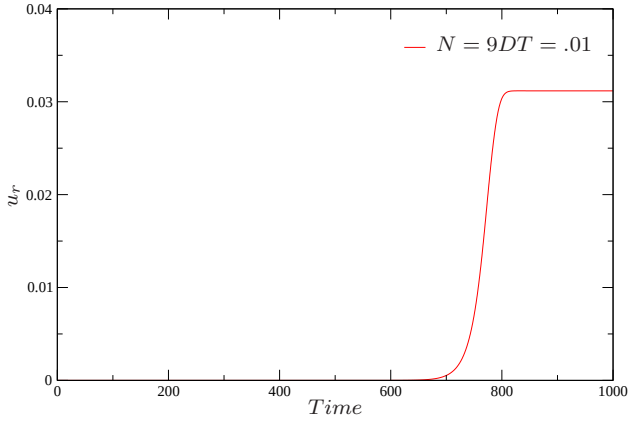

Figure 5: Supercritical u_r, $\eta = .75 \quad Re = 1.01Re_c$

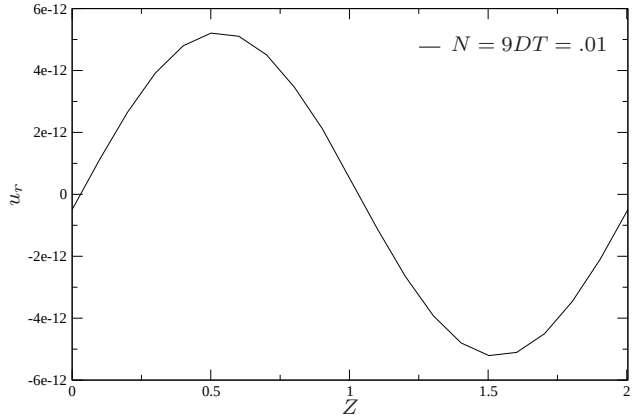

Figure 6: Supercritical u_r down the mid-line, $\lambda = 2.0039$

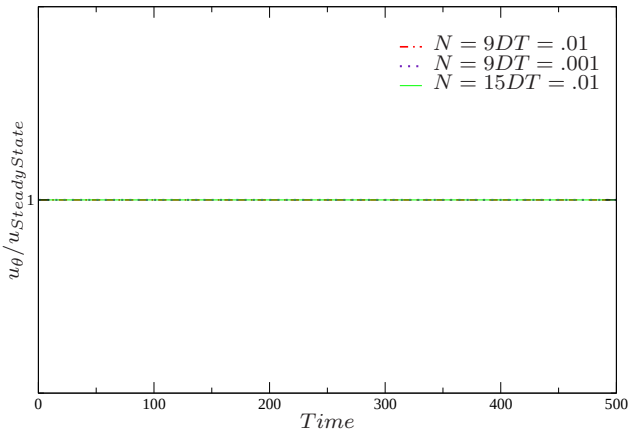

Figure 7: Subcritical u_θ, $\eta = .75 Re = .99Re_c$

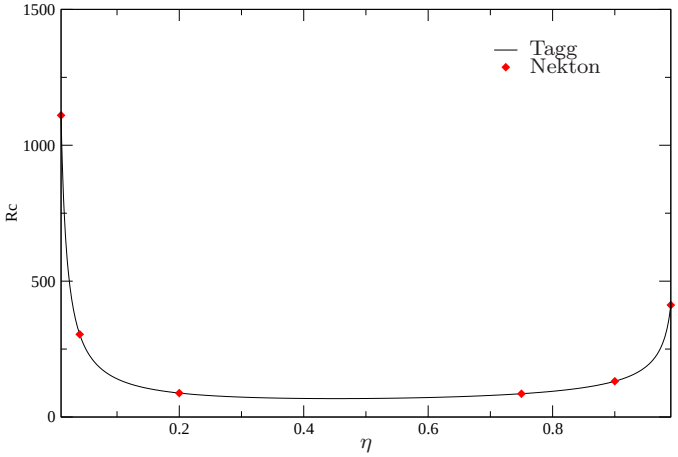

Figure 8: Critical Reynolds number vs η

4.2 Ekman Pumping in an annulus of finite length

In Czarny et al [4], it was verified that TVF occurs below the critical Reynolds number for cylinders of finite length. The TVF is induced by endwall vortices caused by Ekman pumping.

The same discretizations in time and space, as well as polynomial refinement were used for the capped end case with one exception: the velocity profile was "ramped" across the discontinuity where the spinning inner cylinder and the fixed outer wall meet. Our results matched those of Czarny's with only .46% error. It is important that our code verified these results because we will see that Ekman pumping also occurs in our purposed irregular geometry, and that a substantial boundary layer occurs on the lip of the notch.

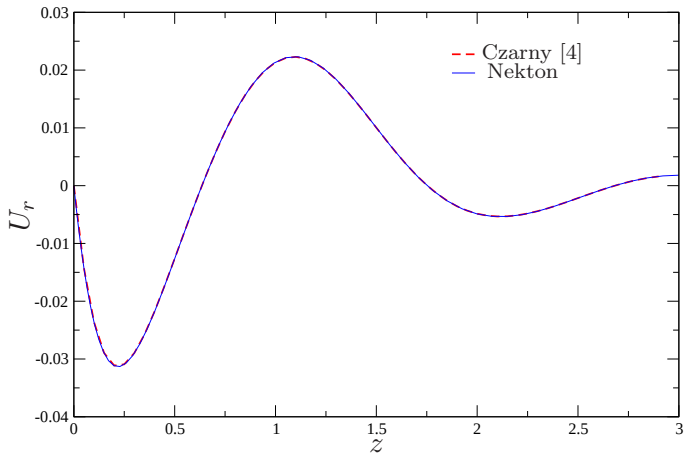

Figure 9: U_r along the midline of finite annulus

Confident that our simulations accurately represent the axisymmetric Navier-Stokes equations in cylindrical coordinates, we proceed into undefined territory.

5 Parallelism and Scaleability

All simulations were run on Hemisphere, a 64-node Beowulf cluster in the Computer Science Department at the University of Colorado at Boulder. Each compute node has dual 2.4GHz Pentium IV Xeon processors and 2GB RAM. To see how well Nek5000 scales for larger jobs we looked at two different metrics for scaleability on this cluster: weak and strong scaling. These tests were performed on the canonical TVF annuli configuration.

In strong scaling, the total work done is kept constant for all runs and on each run the number of processors is doubled. In doing this we expect the amount of time to decrease linearly on a $log2$ scale. For the strong scaling, the simulation was run with a 2000 element mesh, with polynomial degree 15 and a time step of .001. For each configuration the time and operation count is given for 1000 time steps.

# Nodes	# Processors	Total Time (seconds)	# Processors	Total Time (seconds)
2	2	23241.1761	4	15605.9123
4	4	10636.2741	8	8815.8026
8	8	6478.4863	16	3705.4082
16	16	3166.9683	32	2006.1666

While the timing results do not match perfectly with a logarithmic scale, they are nearly exponential with as 2^n. We also note that in comparison, the runs are faster when there are two jobs per node versus only one. This is because we take advantage of the dual processing nodes in the Hemisphere cluster, which saves node-to-node communication time.

Weak scaling requires that the work per node stays the same, so that we scale up work and number of processors equally. Thus, when we double the length of the cylinder, effectively doubling

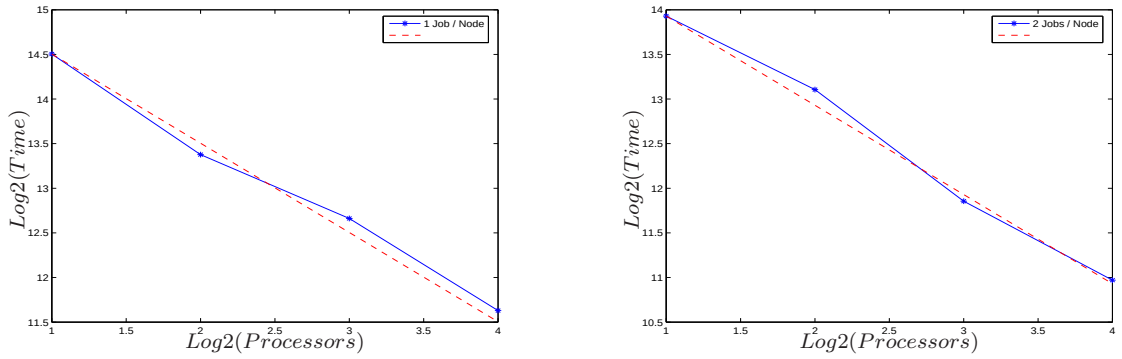

Figure 10: Strong Scaling for 1 job per node and for 2 jobs per node

the mesh, we double the number of processors. What we expect then is that the ratios of the times should be roughly 1. For the weak scaling we chose to utilize the speed of the dual processors by running two processes on each node. All simulations were run with polynomial degree 9 and a time step of .01 for 1000 time steps.

Nodes	Processors	Elements	Run Time (sec)	Setup Time (sec)
1	2	50	26.590	.7985
2	4	100	30.6618	.3497
4	8	200	32.5472	1.493
8	16	400	34.2285	1.3914

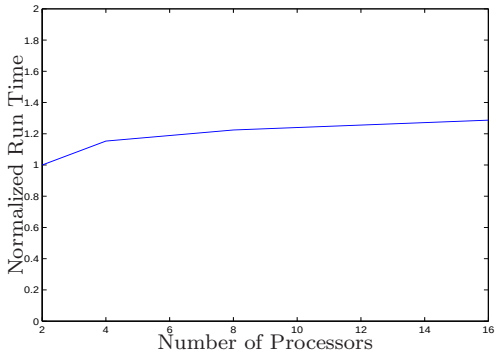

Figure 11: Weak Scaling timing tests

The first thing to note is how quick the runs become with a lower order polynomial refinement, $N = 9$ instead of $N = 15$. We scale the time based on the length of time required to run on two processors and note that the scaled time is roughly constant and close to 1. This means that Nek5000 is not perfectly scaleable, but it is feasible to perform large scale jobs. In the future this testing should be done on larger jobs to examine the asymptotic behavior as $N \to \infty$.

6 Proposed Discontinuous Taylor Couette Problem

In this thesis we examine how vortices between concentric rotating cylinders may be localized in space. P. Weidman has suggested that it should be theoretically possible to tailor vortices to appear at specific locations along the length of the cylinder by altering the geometry of the interior cylinder. Moreover, he suggests that vortices of different wavelengths can be made to appear in

the different sections of the annulus. We will investigate these claims by numerical simulation. By varying the radius ratios $\eta = \frac{R_1}{R_2}$ and $\eta' = \frac{R_1'}{R_2}$ we will simulate three interesting cases,

1. Simultaneous onset of vortices of different wavelengths in the outer and inner region
2. Onset of vortices in the inner section with stable flow in the outer section
3. Onset of vortices in the outer section with stable flow in the inner section

6.1 Geometry

We can do this by introducing a discontinuity in the interior cylinder. Similar to the canonical problem, the outer cylinder is fixed and the interior cylinder is rotating at a constant Ω_1. However, the interior cylinder has a radius R_1 in the notched midsection and a radius of R_1' above and below the midsection.

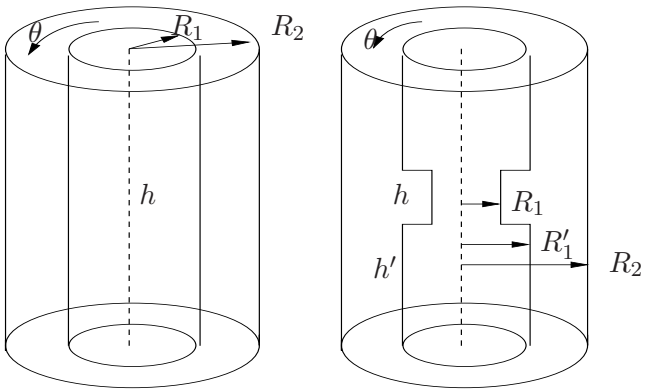

Figure 12: Regular vs Proposed Concentric Cylinder Geometry

The concentric cylinder is broken into an outer region and an inner region. We define the origin at $z = 0$ at the bottom of the inner cylinder and for a nondimensional height h. Written as a function of the radius ratio, the Reynolds number is,

$$R = \frac{\Omega R_1 d}{\nu} = \frac{\Omega R_2^2 \eta(1-\eta)}{\nu}$$

thus for a fixed η, the condition for simultaneous onset of vortices is that of $\eta' = \tilde{\eta}$ where $\tilde{\eta}$ satisfies the relation,

$$\frac{Re_c(\eta)}{\eta(1-\eta)} = \frac{Re_c(\tilde{\eta})}{\tilde{\eta}(1-\tilde{\eta})} \tag{2}$$

Thus, this is how we find our appropriate pairs of (η, η'). By writing R_1, R_1' and R_2 in terms of η, η',

$$R_1 = \frac{\eta}{1-\eta}, \quad R_1' = \frac{\eta'}{1-\eta}, \quad R_2 = \frac{1}{1-\eta}$$

we can define the boundary conditions and initial conditions solely in terms of η, η'.

6.2 Boundary Conditions

The no-slip boundary conditions and initial conditions are defined in terms of $\eta = R_1/R_2$ and $\eta' = R_1'/R_2$. Since we have axisymmetric flow,

$$u_r(r, z, \theta) = u_z(r, z, \theta) = 0, \qquad \text{for all } r, z, \theta$$

To simulate an infinite cylinder we use periodic boundary conditions on the end caps,

$$u_\theta(z=0) = u_\theta(z=h), \qquad \frac{\eta'}{1-\eta} \le r \le \frac{1}{1-\eta}$$

The outer cylinder is stationary,

$$u_\theta = 0.0, \qquad r = \frac{1}{1-\eta} \quad 0 \le z \le h$$

For the interior cylinder we specify Dirichlet boundary conditions,

$$u_\theta = 1.0, \qquad r = \frac{\eta}{1-\eta} \quad 0 \le z \le h$$

For the notch we specify the radial profile,

$$u_\theta = \frac{1-\eta}{\eta} r, \qquad z = h'$$

6.3 Initial Conditions

The steady-state base flow is found in a similar manner to the canonical problem by numerical solution of the Navier-Stokes equations as a function of its angular velocity. The steady-state flow is perturbed with $O(\epsilon)$ random noise.

In the midsection we expect the same profile as we had before,

$$u_\theta = \frac{\eta}{1+\eta}\left[\frac{1}{(1-\eta)^2 r} - r\right] + noise$$

In the upper and lower regions we expect,

$$u_\theta = \frac{\eta'^2}{1-\eta'^2}\left[-\frac{1-\eta}{\eta} r + \frac{1}{\eta(1-\eta)r}\right] + nosie$$

7 Simulations

After examining various coupled values of (η, η'), we were able to gain insight into what could be achieved by altering the interior cylinder with a discontinuous notch. We found that we could in fact tailor the vortices to appear at specific locations along the length of the cylinder. Further, we found that the notch played a significant role in the onset of vortices due to the Ekman pumping. Because of the Ekman Pumping, TVF appears below Re_c in either channel. Thus you cannot produce TVF in one region and CCF in another. However, you can produce a visual difference in stability between the regions. Qualitatively we found that visually, when the difference between (η, η') is large the vortices appearing in the section characterized by the smaller η are significantly smaller than those appearing in the larger η' region. Thus if one were to build and visualize a discontinuous apparatus they should choose (η, η') such that the relative amplitude of the vortices is of the same magnitude. Otherwise, one would never be able to see the smaller vortices in comparison to the larger ones.

Beginning first with close values for (η, η'), we examine the three cases given above with the following mesh and parameters:

Figure(14) Simultaneous onset of vortices of different wavelengths in the outer and inner region is achieved by satisfying equation(2), $\eta = .366 \quad \eta' = .6$, for which $Re_c(\eta) = 69.3021$

Figure(15) Onset of vortices in the inner section with stable flow in the outer section is achieved by increasing η by 5%, $\eta = .3843 \quad \eta' = .6$, for which $Re_c(\eta) = 68.6982$

Figure(16) Onset of vortices in the outer section with stable flow in the inner section is achieved by reducing η by 5%, $\eta = .3477 \quad \eta' = .6$, for which $Re_c(\eta) = 70.1329$

All streamline plots were taken after 5000 time steps of .01 and with a polynomial order of 9.

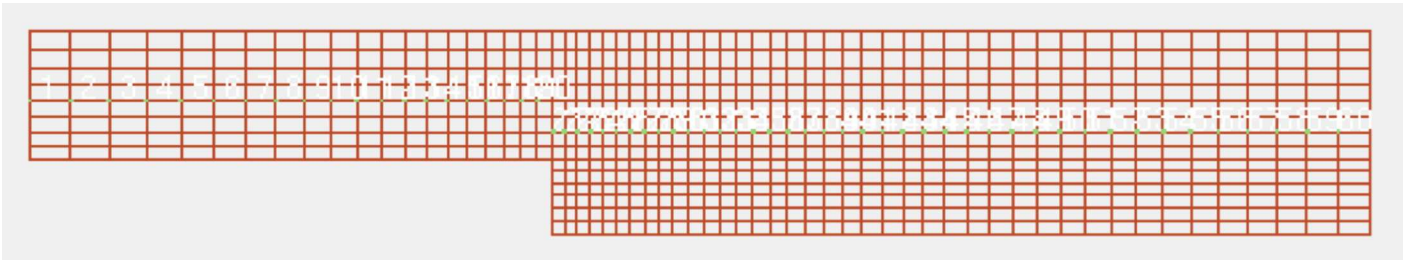

Figure 13: Sample Mesh

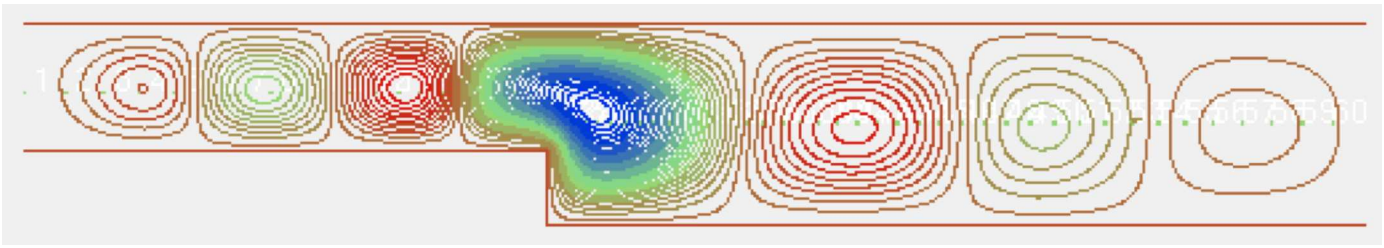

Figure 14: Streamline plot of simultaneous onset of Vortices

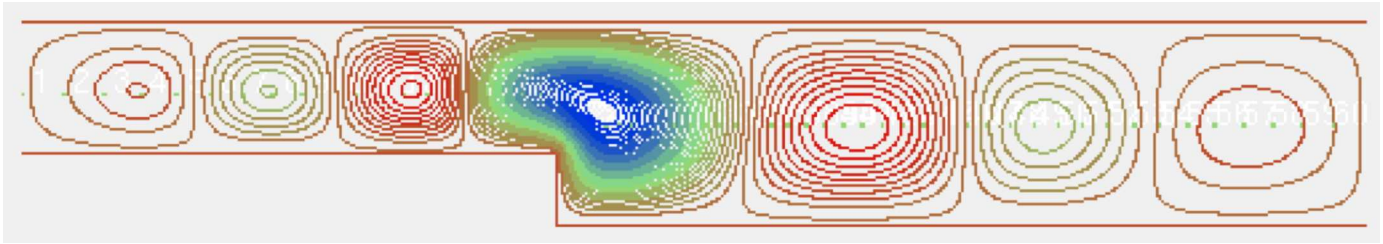

Figure 15: Onset of vortices in the inner section with 'stable' flow in the outer section

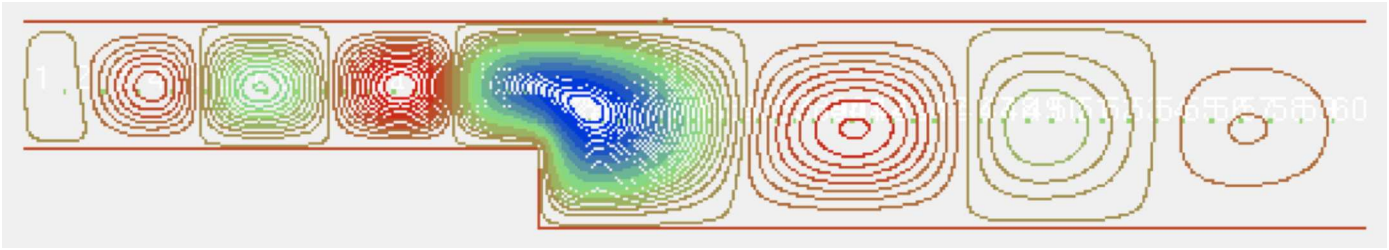

Figure 16: Onset of vortices in the outer section with 'stable' flow in the inner section

What we see in these experiments is that in the 'unstable' regions TVF will appear first and with a larger relative magnitude. However, the discontinuity created by the lip of the notch drives TVF below critical in the regions of 'stability'. We should also note that the vortex on the interface of the discontinuity is made from one vortex from each region and is largest in magnitude no matter the configuration.

For illustrative purposes we now examine values for (η, η') that are far apart. Per P. Weidman's advice we chose to look at the value $\eta = .18939$ which is coupled via equation(2) with $\eta' = .8$. While our previous simulations gave us good insight to the physical characteristics of the discontinuous geometry, finding an appropriate visualization for this pair seemed to be the laborious task. The difficulty in visualizing this particular pair is that for $\eta = .18939$ and $Re = 1.05Re_c$ the max velocity in the radial direction is $O(10^{-11})$. This can be illustrated as follows, in figure(17)

we see that axisymmetric Taylor vortices have set up in the channel, but as we see in figure(18) they are so low amplitude that you see almost no variation in U_θ from CCF.

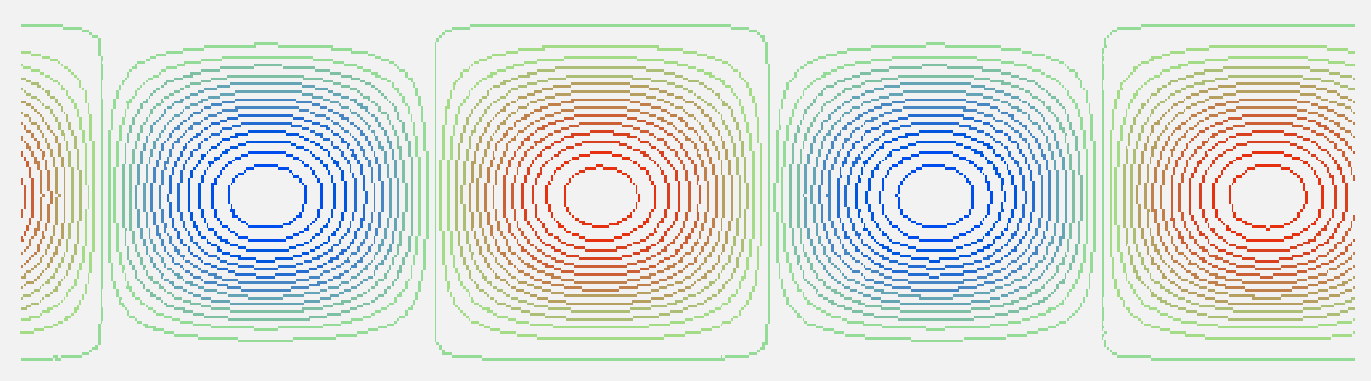

Figure 17: Streamfunction of TVF in Continuous case

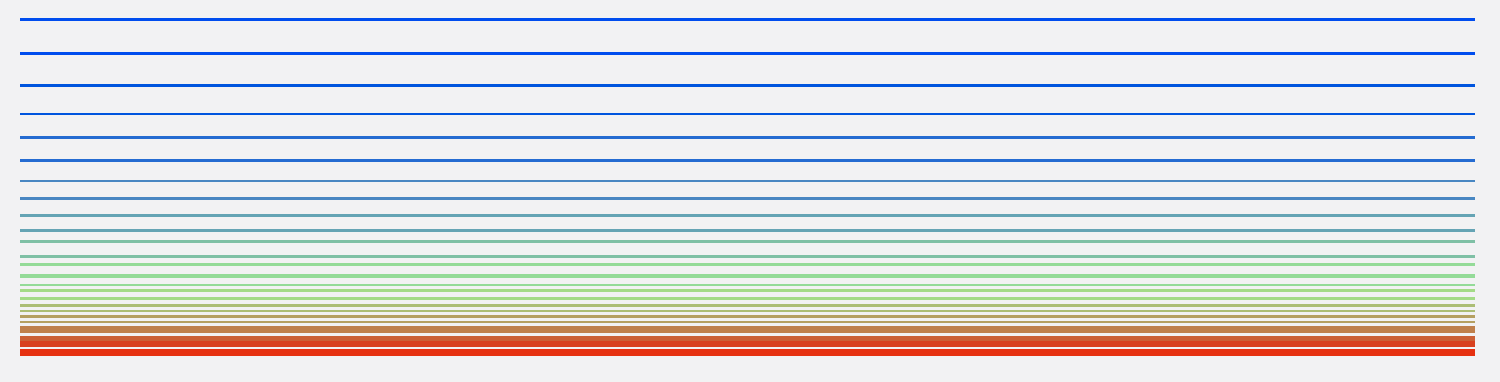

Figure 18: u_θ Profile of TVF in Continuous case

The problem with this is that it makes it difficult to see the onset of vortices in the interior region because of their low amplitude. In figure(19) we compare what TVF looks like in the regular geometry, and note how low the amplitudes of the vortices are. In the second figure we see the large amplitude from the endwall vortex, but everything else is much lower in magnitude and appears irrelevant.

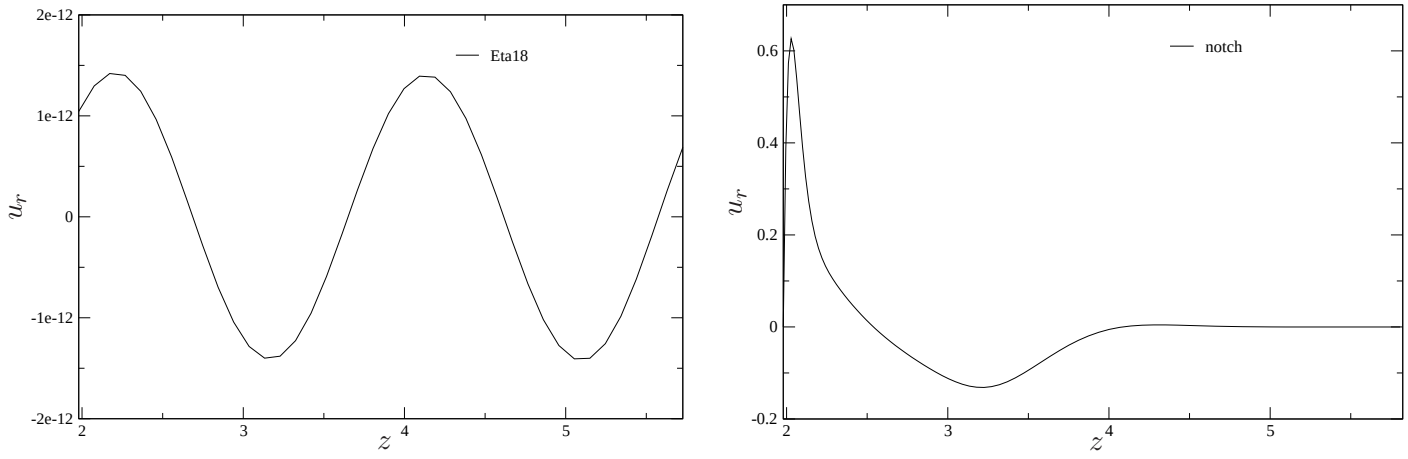

Figure 19: Regular TVF vs TVF in discontinuous geometry

Keeping this in mind we move to examining the three cases previously mentioned, a representative mesh is given below in figure(20). A much more refined mesh was needed in this case because of the non-linear solution to the base flow for the lower eta value .18939

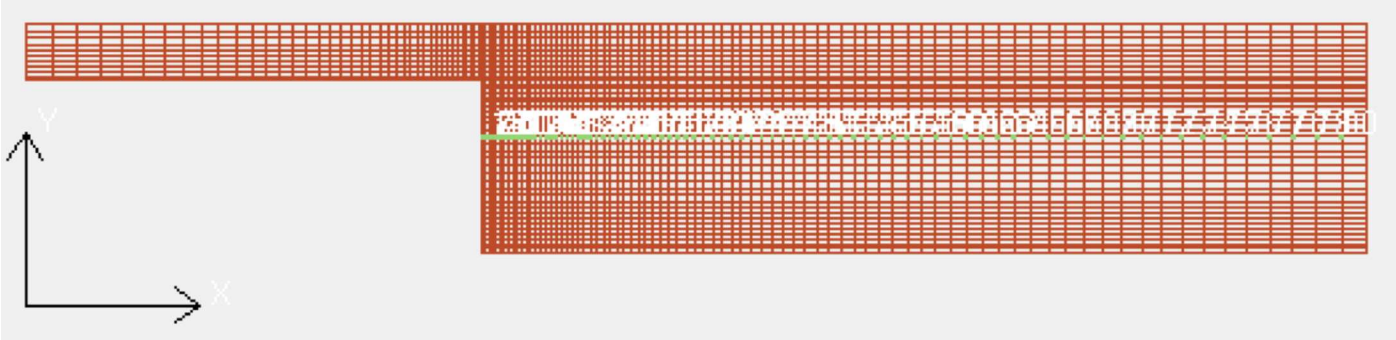

Figure 20: Sample Mesh

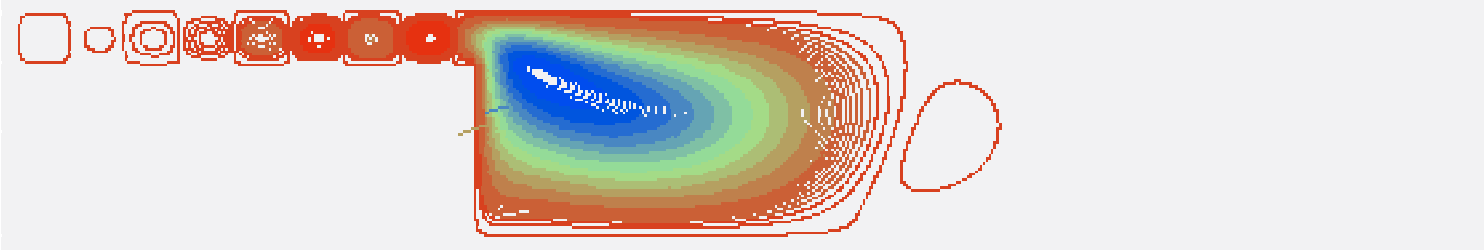

Figure 21: Streamline plot of simultaneous onset of vortices

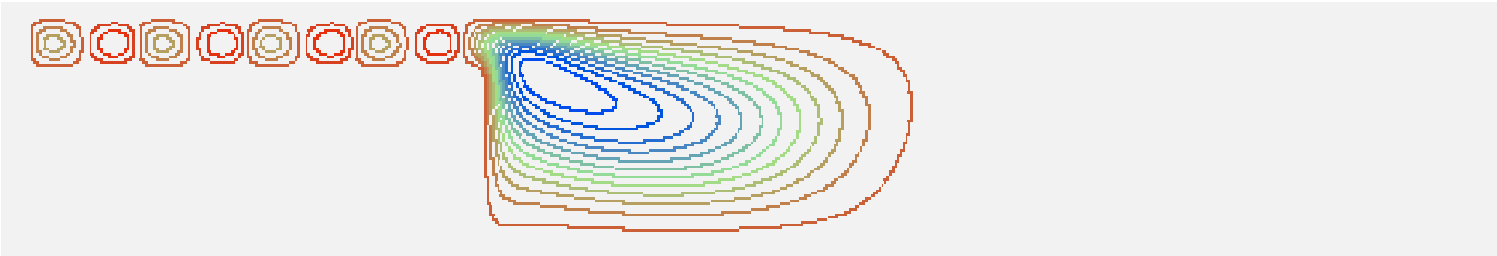

Figure 22: Onset of vortices in the outer section with stable flow in the inner section

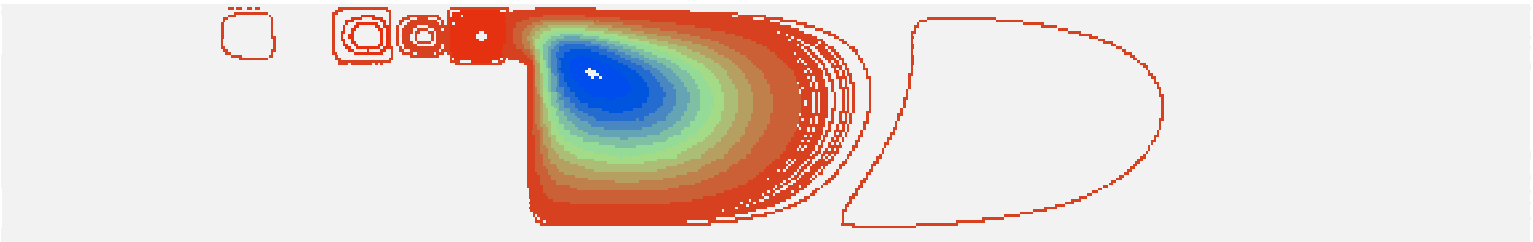

Figure 23: Onset of vortices in the inner section with stable flow in the outer section

What we can see from this is that while in actuality we can create any combination of vortices we like, we must consider the maximum amplitude of the vortices if we want to be able to physically visualize these simulations. We can also see the effect of the length of the notch in relation to how strongly the Ekman pumping forces TVF.

8 Conclusions

In researching CFD, specifically relating to Taylor-Couette Flow, several aspects of the modeling process were explored, including an introduction to the governing equations and their derivations for cylindrical axisymmetric incompressible Navier-Stokes flow, adaptation of the Nek5000 code to simulate axisymmetric flows in 2D and to verification those simulations with published results, and exploration of the effects of geometrical discontinuities of the interior cylinder. It was shown that with careful selection of values for (η, η') one could tailor the appearance, both in amplitude and wavelength, of the TVF in the cylinder. It is anticipated that visually interesting apparatus can be built with the simulated notched geometry. It has been shown that Nek5000 can be used to model the flow near discontinuities in various applications. For, example, one could model the effects of arbitrarily shaped stators relative to the drag they produce. Constructing a display cylinder would be a fun and challenging project because it would require fine-tuning of pertinent parameters in order to effectively tailor the Taylor Vortical Flow into a fine visual presentation!

References

[1] E. Lewis. Steady flow between a rotating circular cylinder and fixed square cylinder. *Journal of the Physical Society of Japan*, 56:855, 1987.

[2] Mullin and A. Lorenzen. Bifurcation phenomena in flows between a rotating circular cylinder and a stationary square outer cylinder. *Phys. Fluids*, 11:1606, 1968.

[3] Mark FL Schumacka and William W. Schultz. Taylor vortices between elliptical cylinders. *Phys. Fluids*, 4(A):2578, 01 June 1992.

[4] Eric Serre, Olivier Czarny, and Patrick Bontoux. Interaction of wavy cylindrical couette flow with endwalls. *Phys. Fluids*, 16(4), April 2004.

[5] H. A. Snyder. Experiments on rotating flows between noncircular cylinders. *Journal of Fluid Mechanics*, 95:497, 1979.

[6] T. Terada and K. Hattori. Formation of vortices by rotating disc, sphere, or cylinder. *Rep. Tokyo Univ. Aeronaut. Res. Inst.*, 2:287, 1926.

[7] H. M. Tufo and P. F. Fischer. Terascale spectral element algorithms and implementations. in Proc. of the ACM/IEEE SC99 Conf. on High Performance Networking and Computing. IEEE Computer Soc., CDROM (1999). http://www.sc99.org/proceedings/tufobell.pdf.

[8] A. P. Willis and C. F. Barenghi. Hydromagnetic taylor■couette flow: numerical formulation and comparison with experiment. *Journal of Fluid Mechanics*, 463:361, 2002.

A Appendix - Steady State CCF

In order to find the solution to the CCF we begin with the axisymmetric Navier-Stokes equation for u_θ in cylindrical coordinates,

$$\frac{\partial u_\theta}{\partial t} + (\mathbf{u}\cdot\nabla)u_\theta + \frac{u_r u_\theta}{r} = \frac{1}{R}\left(\nabla^2 u_\theta - \frac{u_\theta}{r^2}\right) \tag{3}$$

where

$$(\mathbf{u}\cdot\nabla) = u_r\frac{\partial}{\partial r} + u_z\frac{\partial}{\partial z}$$

$$\nabla^2 = \frac{1}{r}\frac{\partial}{\partial r}\left(r\frac{\partial}{\partial r}\right) + \frac{\partial^2}{\partial z^2}$$

For the steady-state case of CCF we solve for u_θ when $\frac{\partial u_\theta}{\partial t} = 0$. Since $U_\theta(r)$ is only a function of r, derivatives of u_θ in θ and z may be dropped. We also note that $u_r = u_z = 0$. These statements collectively reduce the above to the following second order differentiable equation,

$$0 = \frac{\partial^2 u_\theta}{\partial r^2} + \frac{1}{r}\frac{\partial u_\theta}{\partial r} - \frac{u_\theta}{r^2} \tag{4}$$

Which has the general solution,

$$U_\theta = Ar + \frac{B}{r} \tag{5}$$

The no-slip boundary conditions, $U_\theta(r_1) = \Omega_1 r_1$ and $U_\theta(r_2) = 0$ give us,

$$A = \frac{-\Omega_1 r_1^2}{r_2^2 - r_1^2} \qquad B = \frac{(\Omega_1) r_1^2 r_2^2}{r_2^2 - r_1^2} \tag{6}$$

Rewriting r_1,r_2 and Ω_1 in terms of $\eta = r_1/r_2$ we get A and B as follows,

$$r_1 = \frac{\eta}{1-\eta}, \quad r_2 = \frac{1}{1-\eta}, \quad \Omega_1 = 1/r_1 = \frac{1-\eta}{\eta}$$

$$A = \frac{-\eta}{1+\eta} \qquad B = \frac{\eta}{(1-\eta)(1-\eta^2)} \tag{7}$$

which leads to the radial velocity profile,

$$U_\theta = \frac{\eta}{1+\eta}\left[\frac{1}{(1-\eta)^2 r} - r\right]$$

B Appendix - Nek5000

In this appendix we will demonstrate how to simulate 2D flows using NEKTON by exploring axisymmetric flow in cylindrical coordinates, better known as the Taylor-Couette problem. We will also point out a few key parameters of the NEKTON code.

B.1 Axisymmetric Flows

By definition axisymmetric flows in cylindrical coordinates (r, θ, z) have symmetry with respect to θ and thus only depends on (r, z). NEKTON can interpret a two-dimensional Cartesian geometry as the cross section of an axisymmetric body. In this case the axis of rotation is the x axis $\cdots$ i.e. $y = 0$. For purposes of speed, we will do our simulations in two dimensions, with the translation $(x, y) \rightarrow (z, r)$.

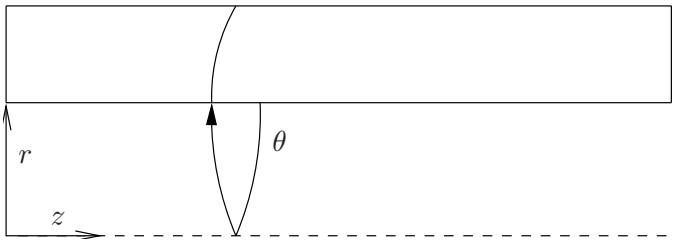

Figure 24: $(x, y) \rightarrow (z, r)$

In NEKTON, axisymmetric flows are assumed to have no azimuthal velocity. In our example of Taylor-Couette flow we do have azimuthal velocity, as the flow is driven by a rotating cylinder. Because of this we have to add an additional equation to represent the missing u_θ terms. The non-dimensional equation for azimuthal flow in cylindrical coordinates is,

$$\frac{\partial u_\theta}{\partial t} + (\mathbf{u} \cdot \nabla) u_\theta + \frac{u_r u_\theta}{r} = \frac{1}{Re} \left(\nabla^2 u_\theta - \frac{u_\theta}{r^2} \right) \tag{8}$$

where the Reynolds number is given as $Re = \frac{LU}{\nu} = \frac{L\Omega r_1}{\nu}$. We can model u_θ by making use of the energy equation and letting temperature model the θ component of velocity. The energy equation in cylindrical coordinates is,

$$\rho c_p \left(\frac{\partial T}{\partial t} + (\mathbf{u} \cdot \nabla) T \right) = k(\nabla^2 T + \frac{T}{r^2}) + q_{vol}$$

letting $T = u_\theta$ and $q_{vol} = -\frac{u_r u_\theta}{r}$ we get,

$$\rho c_p \left(\frac{\partial u_\theta}{\partial t} + (\mathbf{u} \cdot \nabla) u_\theta \right) = k(\nabla^2 u_\theta + \frac{u_\theta}{r^2}) - \frac{u_r u_\theta}{r}$$

and by letting $\rho c_p = 1$ and $k = \frac{1}{R}$ we get,

$$\frac{\partial u_\theta}{\partial t} + (\mathbf{u} \cdot \nabla) u_\theta + \frac{u_r u_\theta}{r} = \frac{1}{R}(\nabla^2 u_\theta + \frac{u_\theta}{r^2})$$

which is the desired model equation for azimuthal velocity. Using temperature to model the radial component of velocity requires some modifications to the code. In *subuser.f* the following changes must be made to the functions *userf* and *userq*.

```
subroutine userf (ix,iy,iz,ieg)
include 'SIZE'
include 'TOTAL'
include 'NEKUSE'
ffx = 0.0
ffy = temp*temp/y
ffz = 0.0

return
```

```
subroutine userq (ix,iy,iz,ieg)
include 'SIZE'
include 'TOTAL'
include 'NEKUSE'
source = 0.0
qvol = - uy*temp/y

return
end end
```

It is very important to realize that further modifications would have to be made if the axis ($y = 0$) were to be included. In the example problem it is not necessary that we consider this case as the interior cylinder is stationary. There are also two versions of *conduct.f*, you should verify that you are using the one set up for axisymmetric problems. The following lines in the original *conduct.f*,

```
cmas CALL AXHELM (TA,T(1,1,1,1,IFIELD-1),H1,H2,IMESH,1)
$ ,IMESH,TOLHT(IFIELD),NMXH,1)
```

should be replaced with

```
cmas CALL AXHELM (TA,T(1,1,1,1,IFIELD-1),H1,H2,IMESH,1)
CALL AXHELM (TA,T(1,1,1,1,IFIELD-1),H1,H2,IMESH,2)
cmas $ ,IMESH,TOLHT(IFIELD),NMXH,1)
$ ,IMESH,TOLHT(IFIELD),NMXH,2)
```

B.2 Parameters

We provide a discussion of some of the most relevant parameters in NEKTON, this is by no means an exhaustive list, for further reference please see the NEKTON manuel. Many of the following comments have been provided by Paul Fisher and Michael Sprague.

DENSITY The density of the fluid or solid. For Boussinesq equations, the recommended value is 1.0.

VISCOS The viscosity. For Boussinesq equations, this is the Prandtl number. When VISCOS is set to a negative value NEKTON is instructed to use the value 1/VISCOS which is the relevant Reynolds number Re. In this case it must be equal to the value given for CONDUCT.

BETAG The product of the volumetric expansion of the fluid with temperature, beta, and the gravitational constant, g.

GTHETA The gravitational acceleration angle in the x-y plane as measured counter-clockwise from the negative y axis (GTHETA = 0.0 is "down"). Note that in order to include the hydrostatic effect, the user still needs to include gravity in the forcing function f.

RHOCP The product of density and specific heat.

CONDUCT The thermal conductivity. When CONDUCT is set to a negative value NEKTON is instructed to use the value 1/CONDUCT which is the relevant Reynolds number Re. In this case it must be equal to the value given for VISCOS.

QVOL A constant volumentric heat source.

FINTIME Stop time if NSTEPS=0.0

NSTEPS The number of steps to use in the simulation if FINTIME=0.0

DTINIT The value of the time step in the simulation. if DT is set to zero, NEKTON automatically (and dynamically) calculates the time step based on the stability requirements imposed on the time step by the Courant condition, or by the stability condition for free surface problems. If DT is set to zero in an unsteady simulation where no stability requirements exist (for flows withough advection, e.g., Stokes flow, or unsteady conduction heat transfer), NEKTON will (arbitrarily) set DT=0.001 in order to proceed with the simulation. In these cases it is therefore stronly reommended th at the user specifies a non-zero DT. If DT is set to a nonzero positive value and the Courant conditions/free surface condition is violated, NEKTON will reduce the time step sufficiently to ensure (temporal) stability. Thus, a nonzero DT positive can be used to define a maximum time step; the actual time step will be either the value of DT specified or a lower value determined by the stability criteria. If DT is set to a negative value the simulation will proceed with a fixed value of DT and the simulation will halt if the Courant condition is violated. If you explicitly choose DT, then set the parameter Courant to reflect the number of sub-steps taken in the characteristics scheme, i.e., Courant=5 would mean 5 substeps. If you do not wish to use the method of characteristics then set IFCHAR=F, and the value specified for Courant will therefore irrelevant. See Courant for further details. It is recommended to begin with a time step of DT=.01 but one should always try reducing their time step to ensure that they have resolved the problem enough.

IOTIME The amount of time between .fld writes; userchk is also called at these intervals.

IOSTEP The number of steps between .fld writes.

INTYPE Flag for solve type for pressure equation 0 - steady, 1 - explicit, -1 - implicit.

NORDER The order of polynomial refinement. This value must match LX1=LY1=LZ1 in SIZEu (which must have been used to compile nek). Defaults to NORDER = 5. Values of 5 - 15 are typical.

DIVERGENCE The convergence criteria for the outer loop (Uzawa, See Section 3.2 of the NEKTON manuel) in the iterative solution of the Stokes equations. The user can directly specify the allowable divergence in the flow field.

HELMHOLTZ The tolerance for the iterative solution of the Helmholtz equation. This stopping criterion applies to the inner elliptic solves in the iterative solution of the Stokes equations, and in the iterative solution of the temperature equation.

NPSCAL The number of passive scalars.

TOLREL The tolerance criterion for velocity errors (relative to the solution velocity) due to incomplete iteration in solving unsteady fluid problems. NEKTON uses this parameter together with the length scales of the problem to calculate eigenvalues, which are then used to convert this physical criterion into numerical convergence criteria for the iterative loops insiede the NEKTON solvers. This ensures optimal efficiency in the NEKTON solvers; the iteration count withing each loop is adjusted separately in order to meet the overall accuracy criterion.

TOLABS This absolute tolerance is used in conjunction with TOLREL described above. NEKTON quits iterating when either the absolute tolerance OR the relative tolerance criterion is satisfied. The strategy for use of these two convergence criteria is illustrated in the following example. For example setting TOLABS=0.01, allows an absolute error of 0.01 in the velocity. Whenever the velocity (norm) is greater than TOLABS (e.g. 0.01), the relative criterion TOLREL will be used. The crierion TOLABS therefore typically applies to the initial time step in order to avoid start-up problems.

Courant The Courant number. Applicable when solving a problem with convection (e.g. Navier-Stokes, forced convection heat transfer, or moving geometry). The convection term is treated explicitly, and the time step must be restricted in order to maintain stability. The maximum allowable time step is proportional to the Courant number; the default value is 0.25 for the standard semi-implicit scheme, and 1.0 if the method of characteristics is used (IFCHAR=T). In the latter case, the user can often acheive further speed-up by increasing the Courant number to about 2 or so. The actual CFL is printed in the logfile at each time step (grep Step logfile, it is the 'C' term). You want to make sure that this term is =< Courant in your code, when using IFCHAR=T, or < .5 when IFCHAR = F. When IFCHAR=F, the time discretization is: BDFk/EXTk-1, where EXTk-1 refers to kth-order extrapolation of nonlinear terms and rhs forcing.

TORDER In a transient simulation, TORDER is the (temporal) order of the multi-step scheme used for the implicit treatment of the diffusion/pressure terms in a fluid problem, or for the implicit treatment of the thermal diffusion a heat transfer problem. TORDER = 1,2,3 refers to a 1st, 2nd, or 3rd order Adams-Bashforth multistep scheme The 1st order scheme is most stable and the 3rd order scheme is least stable. When using the 3rd order scheme it is recommended that the

Also, IFCHAR (T or F) determines whether advection is treated via the so-called characteristics scheme or not. When IFCHAR=T, you can take CFL to be 2 or so. IF IFCHAR = F, then CFL < .5 is standard. Note that if you have significant Coriolois terms (which are treated explicitly) then you may have tighter DT constraints that are not reflected by CFL." Note that for the classical splitting scheme, the temporal order is alsways equal to one.

B.3 Meshing

Meshing can be done inside of PRENEK or with the fortran code *genb6.f*. The fortran code *genb6.f* reads in a file and creates box elements with given dimensions and boundary conditions. When specifying quantities to *genb6.f* you must be careful with white space. For example, it reads 3 spaces for each boundary condition and then looks for a comma so "v,v,v,v" is incorrect while "v ,v ,v ,v" is correctly parsed. An example of a file which can be read into *genb6.f* is given below with its corresponding mesh, see figure(25).

```
base.rea                # base rea file used in generation of parameters for new rea
 2                      # spatial dimension
 2                      # number of fields
 Box 1                  #
 -2 4                   # number of elements in x and y
                        # a negative indicates elements should be automatically placed
                        # otherwise you must give the edges of the elements explicitly
 0.0 2.0 1.0            # dx, places 2 elements evenly spaced (scale 1.0) from 0.0 to 2.0
 0.0 1.0 2.0 3.0 4.0    # dy, places 4 elements at y=0.0, 1.0, ...
 v ,v ,v ,v ,           # BC's
 t ,t ,t ,t ,           # BC's
```

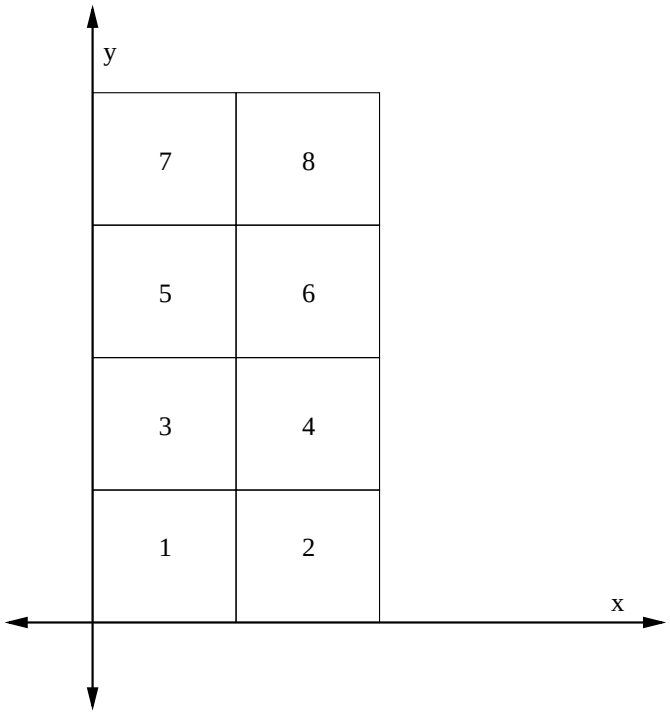

Figure 25: 8 Elements in Box $0.0 \leq x \leq 2.0\,, 0.0 \leq y \leq 4.0$

Meshing can also be done by editing the *.rea* file. In figure(25) element 4's corner points are given in the *.rea* file as,

```
ELEMENT 4 [  1d] GROUP 0
1.00000 2.00000 2.00000 1.00000
1.00000 1.00000 2.00000 2.00000
```

The first row is the x coordinates and the second row is the y coordinates in counter clockwise order. Element boundary conditions are also given in the *.rea* file. Element 4's velocity boundary conditions are given below,

```
E 4 1 2.000000 3.000000 0.000000 0.000000 0.000000
v 4 2 0.000000 0.000000 0.000000 0.000000 0.000000
E 4 3 6.000000 1.000000 0.000000 0.000000 0.000000
E 4 4 3.000000 2.000000 0.000000 0.000000 0.000000
```

For example, the first line indicates that element 4 side 1 has an "element" boundary condition with element 2 side 3. You should verify these boundary conditions against figure(25).

If your problem has discontinuities in its geometry or solution you may want more refinement in that area. You may be tempted to simply add more elements in the area of the discontinuity.

However, when meshing you should try to keep your elements as square as possible in order to keep errors even in x and y. You should also avoid meshes in which an element boundary touches more than one other element boundary, see figure(26). This requires special attention when information is propagated across the boundaries of the conjoining elements. You will see special "join" and "split" boundary conditions appear for these elements. This can cause the code to slow down and error to propagate from the mismatched boundaries.

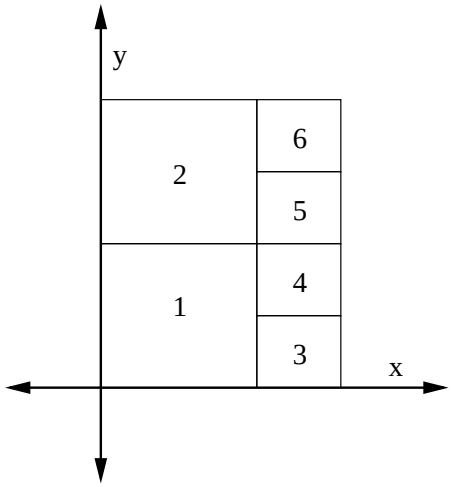

Figure 26: Mismatched Element Boundaries

A better solution would be to scale your elements such that the elements closest to the discontinuity are small. This can be done by changing the scale value in the file given to *genb6.f*. In figure(27) the four elements in x are placed automatically with a scale of 1.5. In this manner you

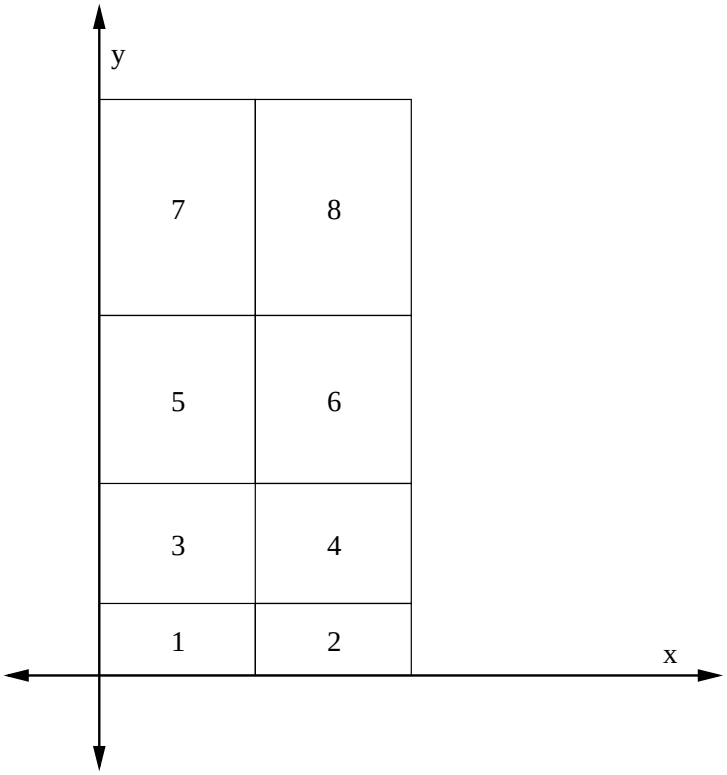

Figure 27: Scaled Elements

can place a finer grid spacing near sharp gradients which require more resolution.

B.4 Boundary and Initial Conditions

Boundary conditions are specified during PRENEK or explicitly in the *.rea* file. While there are many boundary conditions you will be most likely to use either velocity 'v', periodic 'P' or symmetry 'SYM'. Velocity boundary conditions can either be constants or user defined functions. If you have non-constant boundary conditions NEKTON will look to, `subroutine userbc` in the *.usr* file for definitions of the relevant boundary conditions. NEKTON also looks to, `subroutine useric` for definitions of relevant initial conditions. If you generate your boundary and initial conditions through PRENEK it will generate the appropriate code for these two functions.

Another thing to consider are discontinuities in your geometry or solutions. If you have for example a discontinuity across an element you may want to smooth the boundary conditions appropriately.

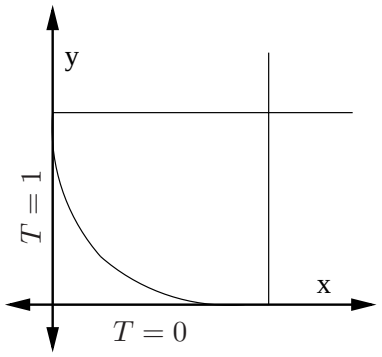

Figure 28: Ramped Boundary Conditions Over a Discontinuity